Microwave-induced activation of additional active edge sites on the MoS_2 surface for enhanced Hg^0 capture

Haitao Zhao[1,2], Xueliang Mu[1], Gang Yang[1], Chengheng Zheng[2] Chenggong Sun[3], Xiang Gao[2,], Tao Wu[1,4,*]*

[1]Municipal Key Laboratory of Clean Energy Conversion Technologies, The University of Nottingham Ningbo China, Ningbo 315100, P. R. China

[2]College of Energy Engineering, Zhejiang University, Hangzhou 310027, P. R. China

[3]Department of Chemical and Environmental Engineering, The University of Nottingham, Nottingham NG7 2RD, The UK

[4] New Materials Institute, The University of Nottingham Ningbo China, Ningbo 315100, P. R. China

Corresponding author: tao.wu@nottingham.edu.cn; xgao@zju.edu.cn

Abstract

In recent years, significant effort has been made in the development of novel materials for the removal of mercury from coal-derived flue gas. In this research, microwave irradiation was adopted to induce the creation of additional active sites on the MoS_2 surface. The results showed that Hg^0 capture efficiency of the adsorbent containing MoS_2 nanosheets being microwave treated was as high as 97%, while the sample prepared via conventional method only showed an efficiency of 94% in its first 180 min testing. After the adsorbent was treated by microwave irradiation for 3 more times, its mercury removal efficiency was still noticeably higher than that of the sample prepared via conventional method. Characterization of surface structure of the MoS_2 containing material together with DFT study further revealed that the (001) basal planes of MoS_2 crystal structure were cracked into (100) edge planes (with an angle of approximately 75 degrees) under

microwave treatment, which subsequently resulted in the formation of additional active edge sites on the MoS_2 surface and led to the improved performance on Hg^0 capture.

Keywords: MoS_2 surface, mercury capture, microwave irradiation, additional active edge site

1. **Introduction**

Mercury (Hg) has become a global concern due to its significant negative impacts on human being's health and the environment [1], the potential for long-range atmospheric transport, the possibility for bio-accumulation in ecosystems, and the persistence in the environment [2]. Therefore, 42 nations (128 signatories) have joined the Minamata Convention on Mercury aiming at reducing global anthropogenic mercury emissions [3, 4]. The recent Global Mercury Assessment showed that the combustion of coal is one of the largest anthropogenic sources of mercury emission and accounts for the emission of approximately 475 tonnes of mercury per annum [5]. During coal combustion process, mercury is emitted into the air in three forms: elemental (Hg^0), oxidised (Hg^{2+}), and particle-bound ($Hg^{(p)}$) [6]. Elemental mercury, which accounts for about 80 % of the total mercury emission, is extremely difficult to be removed from flue gas by those existing air pollution control devices at coal-fired power stations [7].

Due to the ever-tightening legislations on Hg^0 emission [8, 9], in recent years, there have been considerable interests in the development of technologies for the removal of Hg^0 in coal-derived flue gas. Among these technologies, activated carbon injection (ACI) has been commercially deployed since 2005 for the removal of Hg^0 at coal-fired power plants [10-12]. It is found that mercury removal capacity of activated carbon can be enhanced by impregnating with sulphur due to the high affinity of sulphur to mercury, which results in the formation of stable mercury sulphides [13, 14]. However, the activated carbon injected for the adsorption of mercury might

compromise fly ash as a saleable by-product [15-17]. It is therefore essential to develop alternative non-carbon-based solid sorbents for mercury removal [18-22].

Compared with sulphur impregnated activated carbon, the graphene-like transition-metal dichalcogenides (TMDs) have demonstrated great potential for Hg^0 capture due to the surface being functionalized with ultra-abundant sulphur [23]. In our previous study [24], it was found that the removal of Hg^0 at low temperatures was achieved via the immobilization of Hg atoms with sulphur atoms on the entire basal plane of the MoS_2 surface. The recent study demonstrated that the cracking of the basal plane of the surfaces could result in the formation of additional active edge sites by adjusting the concentration of precursors and therefore improve the performance of the electrocatalytic hydrogen evolution [25]. In addition, it is found that the edge sites (or defects) of two dimensional materials are crucial for many applications such as oxygen reduction reaction, hydrogen evolution reaction, oxygen evolution reaction and overall water splitting [26-29]. Nevertheless, the creation of additional active edge sites by microwave irradiation and its effect on Hg^0 capture performance remain unexplored.

Due to the unique features of microwave irradiation, such as volumetric and selective heating, there are growing interests in the use of microwave for material synthesis and in the utilization of microwave to enhance process conversion/selectivity [30, 31]. In recent years, microwave has also been successfully applied in the preparation of high-quality graphene [32], graphene on Cu foils [33], nitrogen doped graphene [34] and graphene hybrid aerogels [35], etc. However, the use of microwave irradiation to prepare graphene-like MoS_2 with edge planes for Hg^0 removal has not yet been investigated.

Therefore, the objective of this study was to apply microwave irradiation to create additional active edge sites on the MoS_2 surface and subsequently enhance the performance of MoS_2 in Hg^0 capture.

Materials characterization, Hg^0 capture performance testing as well as theoretical study based on DFT modeling were carried out to reveal the process of the creation of additional active sites and how it contributed to the enhanced Hg^0 capture performance.

2. Materials and methods

2.1 Preparation of samples

The incipient wetness impregnation (IWI) method followed by sulfur-chemical vapour reaction (S-CVR) was adopted for the preparation of MoS_2 adsorbent (approximately 16.0 grams per batch) on a γ-Al_2O_3 support (V-SK Co., Ltd., size range: 1.18 mm $\leq$ x $\leq$1.70 mm, surface area: 188 m^2/g), followed the procedures described elsewhere [24]. Characteristic of this MoS_2-containing material can be found in our previous research [24].

2.2 Microwave treatment of samples

In this research, microwave-induced activation (MW-IA) was tried as a means to create additional active sites. A single mode microwave cavity was designed and used in this study to active the MoS_2 surfaces containing adsorbent (approximately 2.0 grams, which was prepared previously using conventional heating) in N_2 gas at a flow rate of 1500 ml/min (1kW microwave power input, 2450 MHz). The MW-IA reactor was operated in a temperature control mode and the temperature was set as 200 °C. For comparison purposes, the same sample was also tested at the same temperature and gas atmosphere conditions under conventional heating in an electric furnace.

2.3 Measurement of Hg^0 capture performance

Gas phase Hg^0 was generated by using a mercury generator (Tekran 2537, USA). The measurement of Hg^0 capture performance was conducted in an experimental system consisting of

two reactors placed in parallel in the single mode microwave cavity or the electric furnace. The concentration of Hg^0 at the inlet and outlet was monitored by using the mercury analysis system (Tekran 3300RS, USA, detection limit < 0.05 μg/m^3). The experimental procedures are described elsewhere [24, 36].

2.4 Raman Spectroscopy

Raman spectra of the samples were analyzed using a Raman Renishaw RM2000. The pump radiation was supplied by a 514 nm diode laser and the Raman emission was focused through a 50 × objective [37].

2.5 Morphology of samples

A high-resolution transmission electron microscopy (HRTEM, JEM 2100) was used to characterize morphology of the samples [38] , which was operated at 200 kV. This is to show the existence of different MoS_2 structural features.

2.6 DFT modeling

All calculations were performed using the Density Functional Theory – Dispersion Correction (DFT-D) with exchange-correlation functional GGA-PW91-OBS [39]. All possible ion-electron interactions were considered in the system with the **U**ltra**S**oft **P**seudo**P**otentials (USPP) implemented [40]. An energy cutoff of 310 eV and 2×2×1 k-points mesh using the method of Monkhorst–Pack was chosen to ensure that the total energy of MoS_2 surface is converged within 1×10^{-5} eV/atom [41]. In the DFT modeling, the maximum force was within 0.03eV/Å; the maximum stress was within 0.05 GPa; and the maximum atom displacement was within 0.001 Å. In order to optimize the stable configuration of MoS_2 surface and the adsorbate-covered MoS_2 surface, a vacuum region of 25 Å was also applied in the direction perpendicular to the MoS_2

surface.

The adsorption energy, E_{ad}, was calculated by

$$E_{ad} = E_{Hg+MoS_2} - (E_{Hg} + E_{MoS_2}) \quad (1)$$

where E_{Hg} is the ground state energy of the free Hg atom in a (11 Å) ^{3} supercell; E_{MoS_2} is the total energy of the free MoS_2 surface, and E_{Hg+MoS_2} is the total energy of the Hg atoms being adsorbed on the MoS_2 surface in the optimized system.

3. Results and discussion

3.1 Performance of the MW-IA treated sample

In this research, the Hg^0 capture performance of the MW-IA treated MoS_2 was studied and was compared with those treated following conventional heating method, the results of which are plotted in Figure 1.

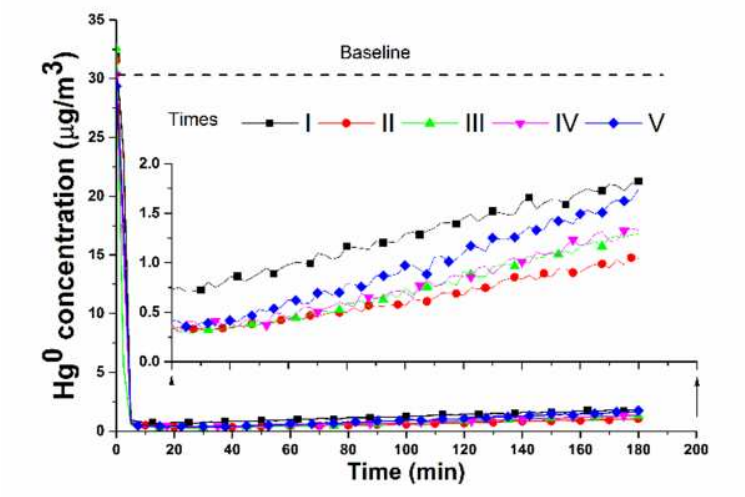

Figure 1 Enhanced Hg^0 capture of the MoS_2-containing adsorbents before and after MW-IA treatment

The Test I was for the MoS_2-containing adsorbent that was prepared under conventional heating, which showed a Hg^0 removal efficiency of 94 wt% after a 3 h testing. By contrast, for the

adsorbents after MW-IA treatment (Tests II-V), better Hg^0 removal performance was observed. The mercury removal efficiency was around 97 wt% and 96 wt% for the same adsorbent being MW-IA treated for once (Test II) and twice (Test III) in Figure 1, respectively. In addition, the Hg^0 removal performance of the adsorbents being MW-IA treated for three (Test IV) and four (Test V) times was still noticeably better than that of the sample prepared via conventional heating method. These results suggest that the MW-IA treatment might lead to the formation of more active sites available for the adsorption of more Hg atoms.

The main reasons for the formation of additional active sites after microwave irradiation might be attributed to the volumetric, uniform and selective heating nature of microwave, which caused beneficial changes in the physical and chemical properties of the MoS_2 surface. These changes may subsequently favor the chemical adsorption of Hg atoms, allowing more Hg atoms to be adsorbed onto the surface with additional active sites. However, the mechanism of this interesting phenomenon is still unknown. Therefore, detailed surface characterizations and theoretical study was further carried out in this study to reveal the mechanism of such enhancement in Hg^0 capture.

3.2 Characterizations of MoS_2 surface modification

To examine the changes on the MoS_2 surface-containing adsorbent treated by the MW-IA approach, a series of characterizations were carried out in this study.

The number of S-Mo-S layers of the samples was characterized by Raman spectroscopy. As shown in Figure 2, there are two strong peaks at the in-plane E^1_{2g} and the out-of-plane A_{1g} vibration (schematic diagrams is also shown in the embedded figures) in the Raman spectra, which locate at around 382 cm^{-1} and 405 cm^{-1}, respectively. Normally, the number of layers of original materials can be identifed based on the peaks of E^1_{2g} and A_{1g} [42]. Compared with peak intensity of the

adsorbent processed by conventional heating treatment, the intensity of microwave irradiation treated materials significantly increased after MW-IA treatment. It can be concluded that the interlayer interactions became stronger with the additional layers [43].

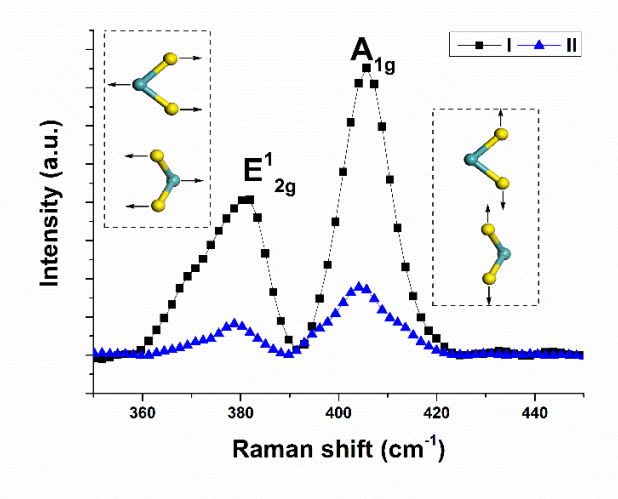

Figure 2 Raman spectroscopy of the adsorbents processed by microwave-induced activation (I) and conventional heating (II). (Embedded left figure: schematic diagram of in-plane vibration. Embedded right figure: schematic diagram of out-of-plane vibration.)

To further prove this phenomenon, the sample after MW-IA treatment was studied by using HRTEM as shown in Figure 3. Characteristic fringes are obvious in the HRTEM image. The interplanar spacing of approximately 0.63 nm is identifiable in the image, which is the characteristic pattern of (100) edge plane of (002) MoS_2 crystal structure. Moreover, an interplanar spacing around approximately 0.27 nm, which is the characteristic pattern of (001) basal plane of (100) MoS_2 crystal structure, is also identifiable in the HRTEM image. This pattern is similar as what was observed on the MoS_2 containing adsorbent (without MW-IA treatment) in our previous report [24]. These results suggest that during the course of MW-IA treatment, a portion of the (001) basal planes of MoS_2 crystal structure were cracked to (100) edge planes (along an angle of

approximately 75 degrees) and thus resulted in the formation of additional edge planes for enhanced Hg^0 uptake. Based on these observations, the schematic diagram of the cracking process is proposed and illustrated in Figure 3 (b). This is in good agreement with the recent findings reported in the study of electro-catalytic hydrogen evolution [25]. Therefore, it is believed that additional active edge sites were created by the MW-IA treatment, which subsequently enhanced the Hg^0 capture performance.

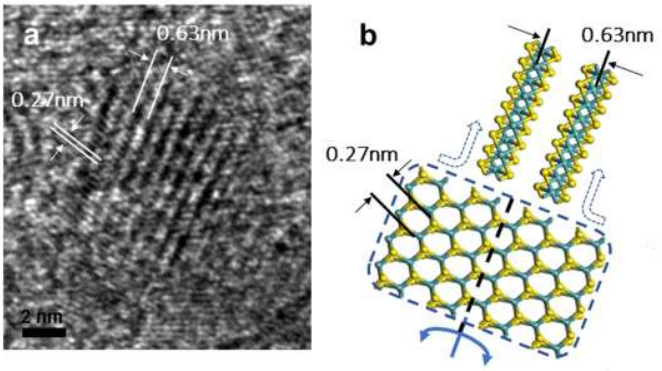

Figure 3 (a) High-resolution electron microscopy (HRTEM) image of the adsorbent processed by the MW-IA treatment. (b) Schematic diagram of the cracking process under MW-IA treatment

3.3 Interactions between Hg atoms and MoS_2 surface

The formation of additional active sites for the enhanced Hg^0 uptake was further proved by the DFT-D calculation by comparing the inside interactions of Hg^0 with the basal plane and the edge plane of the MoS_2 surface. Based on the full optimizations, the adsorption energy (E_{ad}) was identified as an indicator to evaluate the potential of various possible Hg^0 adsorption sites. Three stable adsorption configurations were identified on the MoS_2 (001) surface and the two sides of the MoS_2 (100) surface. There are Hg atoms being adsorbed on top of the hollow space among the

neighboring sulfur atoms above the S covered side of the MoS_2 (100) surface (H_S position) and on top of the hollow space among the neighboring Mo atoms above the Mo covered side of MoS_2 (100) surface (H_{Mo} position), and on top of Mo atoms with a three-fold binding to the neighboring sulfur atoms above MoS_2 (001) surface (T_{Mo} position), as shown in Figure 4 (a), 5 (a) and 1S (a), respectively.

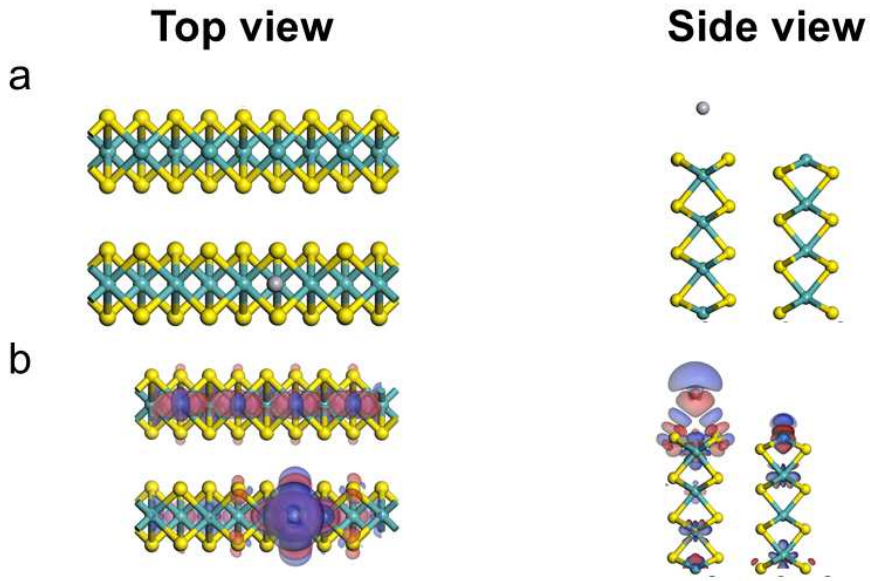

Figure 4. (a) Optimized structure of the H_S adsorption position on the MoS_2 (100) surface and (b) the corresponding charge density difference analysis of an Hg atom being adsorbed on the MoS_2 (100) for the H_S adsorption position configuration (The red (blue) distribution corresponds to charge depletion (accumulation). Isosurface is 0.001 e/ $Å^3$).

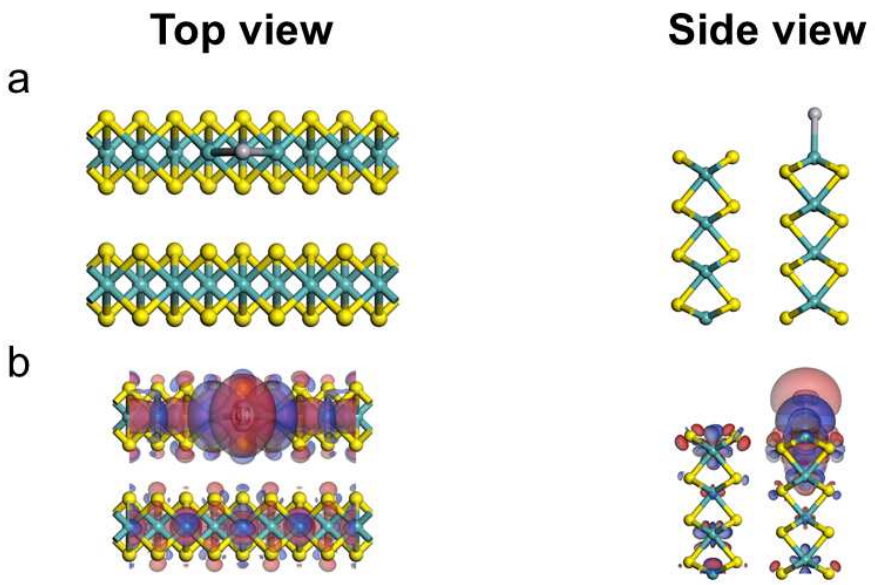

Figure 5. (a) Optimized structureswith H_{Mo} adsorption position on the MoS_2 (100) surface and (b) the corresponding charge density difference analysis of an Hg atom being adsorbed on the MoS_2 (100) for H_{Mo} adsorption position configuration (The red (blue) distribution corresponds to charge depletion (accumulation). Isosurface is 0.001 e/ Å^3).

According to Equation 1, the stability of the adsorption configuration was found to be in the order of H_{Mo} > H_S > T_{Mo} as listed in Table 1. All three adsorption positions demonstrated adsorption energy that allows Hg atoms to be chemically adsorbed on the MoS_2 surface [44]. Compared with the T_{Mo} position on the MoS_2 (001) surface, there is a larger absolute adsorption energy for the H_S position on the Sulphur covered side of the MoS_2 (100) surfaces with a shorter d(Hg-S_{NA}) (i.e., the distance between the Hg atom and the nearest adjacent (NA) S atoms) and the lower δ%(Hg-S_{NA}) (i.e., the percentage of the d (Hg-S_{NA}) vs the covalent bond of Hg-S) as shown in Table 1. In addition, the H_{Mo} position on the Mo atoms covered side of the MoS_2 (100) surfaces has the most negative adsorption energy (i.e., -2.801 eV) with the shortest d(Hg-Mo_{NA}) (i.e., the distance between the Hg atom and the NA Mo atoms) (2.95 Å) and the lowest δ%(Hg-Mo_{NA}) (9.89%). The

above geometric results of the adsorption configuration further confirmed that the main interaction between the Hg atom and the MoS_2 surface is chemisorption [45]. Therefore, the edge plane of the MoS_2 (100) shows stronger ability in attracting Hg atoms, which is contributed by both the S and Mo atoms on the MoS_2 (100) surface, than that of the basal plane of the MoS_2 (001) surface.

Table 1 Adsorption properties of an Hg atom on a stable adsorption configuration of the MoS_2 (100) surface and the MoS_2 (001) surface

Position	E_{ad}[1] (eV)	d(Hg-S $_{NA}$)[2] (Å)	d(Hg-Mo $_{NA}$)[3] (Å)	δ% (Hg-S $_{NA}$)[4]	δ%(Hg-Mo $_{NA}$)[5]
T_{Mo}	-1.125	3.90	5.05	58.06%	88.47%
H_S	-2.165	3.44	4.33	39.27%	61.64%
H_{Mo}	-2.801	3.67	2.95	45.63%	9.89%

(Note: 1, adsorption energy. 2, optimized distance between a Hg atom and the NA S $_{NA}$ atoms. 3 optimized distance between a Hg atom and the Mo $_{NA}$ atom, 4, the percentage of covalent bond vs the distance between the Hg atom and the S $_{NA}$ atom for Hg adsorption on different positions, 5, the percentage of covalent bond vs the distance between a Hg atom and the Mo $_{NA}$ atom for Hg adsorption on different positions)

The mechanism of Hg^0 captured on the different MoS_2 surfaces was further studied by charge density difference analysis and PDOS analysis. The plots of the charge-density difference for Hg^0 adsorption on the H_S position, the H_{Mo} position of the MoS_2 (100) surface and the T_{Mo} position of the MoS_2 (001) surface, are shown in Figure 4 (b), 5 (b) and 1S (b). These figures further indicate that Hg atoms are chemically adsorbed on the surface and there is a clear chemical bonding between the Hg atom and the Mo atom at the H_{Mo} position on the MoS_2 (100) surface. Charge transfer for the Hg atoms adsorbed on the most stable adsorption configuration on the MoS_2 (100) surface and (001) surface was further calculated by Hirshfeld method as summarized in Table 1S.

The amount of donating electrons of Hg atoms at the H_{Mo} position is 10 times greater than those of the T_{Mo} position.

To further understand interactions of the orbitals of the Hg atom with the H_{Mo} position of the MoS_2 (100) surface, the partial density of states (PDOS) of the surface atoms was investigated from the atomic view as shown in Figure 6.

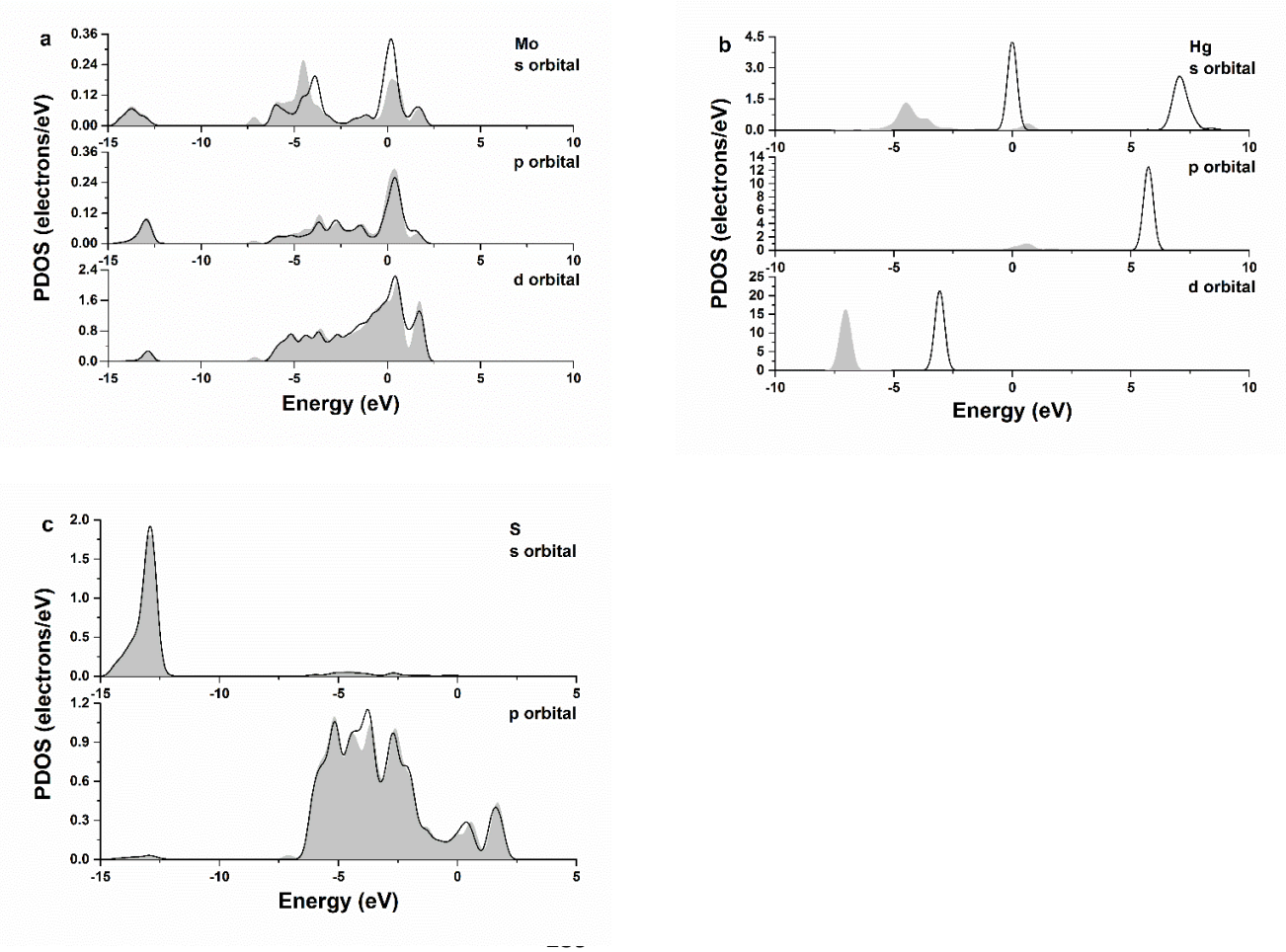

Figure 6. PDOS analysis of a Hg atom and its adjacent Mo and S atoms on the H_{Mo} position of MoS_2 (100) surface. (a) PDOS of s, p and d orbital for the Mo $_{NA}$ atom. (b) PDOS of s, p

and d orbital for an isolated Hg atom. (c) PDOS of s and p orbital for the S_{NA} atom. (Black line represents before adsorption, the grey shadow represents after adsorption).

When compared with the PDOS of the T_{Mo} position on the MoS_2 (001) surface (in Figure 2S), the PDOS peaks of d, s and p orbitals of an isolated Hg atom on MoS_2 (001) and MoS_2 100) are near -3.1, 0 and 5.7eV before adsorption, respectively. After adsorption, all the PDOS peaks of the Hg atom shifted left with the state of s and p orbitals significantly decreased in energy level, which suggests strong interactions between the Hg atom and the MoS_2 (001) and (100) surfaces. However, only the s orbital of PDOS peak of the Mo atom shifted left on the MoS_2 (100) surface after adsorption, which is caused by the transfer of electrons from s orbital of the Hg atom to the s orbital of the Mo atom. Therefore, the edge sites in MoS_2 surfaces have stronger interactions with Hg atoms than that of the original adsorbent, because of the additional active adsorption sites (edge sites) created after MW-IA treatment.

4. Conclusions

In this research, it is demonstrated that Hg^0 capture performance of the MoS_2 adsorbent being MW-IA treatment is better than that of the adsorbent prepared via conventional heating method. The characterization showed that the (001) basal planes of the MoS_2 crystal structure were cracked into (100) edge planes (with an angle of approximately 75 degrees) during the MW-IA treatment and thus resulted in the formation of additional active edge sites, which subsequently contributed to the enhanced Hg^0 removal efficiency. The DFT modelling further proved that Hg^0 capture ability was enhanced by the sulfur and the Mo atoms on the MoS_2 (100) surface, which contributed to higher adsorption energy for the H_{Mo} site than that of the sites on the MoS_2 (001) surface. Therefore, it is demonstrated the microwave induced activation (MW-IA) treatment can be used

to create additional active edge sites on the MoS_2 surface to further improve Hg^0 capture performance.

Acknowledgments

China Postdoctoral Science Foundation (2016M601942) and Ningbo Bureau of Science and Technology (Innovation Team Scheme, 2012B82011) are acknowledged for partially sponsoring this research. The University of Nottingham Ningbo China (UNNC) is acknowledged for the provision of a full scholarship to the 2nd author. UNNC IT services team is also acknowledged for the IT support.

References

1. Ling, L., et al., *Effects of metals doping on the removal of Hg and H2S over ceria.* Applied Surface Science, 2017. **403**: p. 500-508.
2. Xie, Y., et al., *Experimental study on Hg0 removal from flue gas over columnar MnOx-CeO2/activated coke.* Applied Surface Science, 2015. **333**: p. 59-67.
3. UNEP, *Minamata Convention on Mercury [Online] available from <www.mercuryconvention.org> (accessed Dec 01, 2016)*. 2013: Switzerland.
4. Zhang, X., et al., *Simultaneous removal of elemental mercury and NO from flue gas by V2O5–CeO2/TiO2 catalysts.* Applied Surface Science, 2015. **347**: p. 392-400.
5. UNEP, *Global Mercury Assessment 2013: Sources, emissions, releases, and environmental transport [Online] available from <http://www.unep.org> (accessed Jan, 2017)*. 2013.
6. Geng, L., et al., *A first-principles study of Hg adsorption on Pd(1 1 1) and Pd/γ-Al2O3(1 1 0) surfaces.* Applied Surface Science, 2014. **321**: p. 30-37.
7. Jungsuttiwong, S., et al., *Density functional theory study of elemental mercury adsorption on boron doped graphene surface decorated by transition metals.* Applied Surface Science, 2016. **362**: p. 140-145.
8. EPA-US, *Mercury and Air Toxics Standards (MATS) for power plants. http://www.epa.gov/mats/actions.html*. 2011.
9. MEP-China, *Emission standard of air pollutants for thermal power plants (GB 13223-2011) (In Chinese)*. 2011.
10. Sjostrom, S., et al., *Activated carbon injection for mercury control: Overview.* Fuel, 2010. **89**(6): p. 1320-1322.
11. Meeprasert, J., et al., *Capability of defective graphene-supported Pd13 and Ag13 particles for mercury adsorption.* Applied Surface Science, 2016. **364**: p. 166-175.
12. Rupp, E.C. and J. Wilcox, *Mercury chemistry of brominated activated carbons – Packed-bed breakthrough experiments.* Fuel, 2014. **117, Part A**(0): p. 351-353.
13. Yao, Y., V. Velpari, and J. Economy, *Design of sulfur treated activated carbon fibers for gas phase elemental mercury removal.* Fuel, 2014. **116**(0): p. 560-565.

14. Saha, A., et al., *An X-ray Photoelectron Spectroscopy Study of Surface Changes on Brominated and Sulfur-Treated Activated Carbon Sorbents during Mercury Capture: Performance of Pellet versus Fiber Sorbents.* Environmental Science & Technology, 2013. **47**(23): p. 13695-13701.
15. Aboud, S., E. Sasmaz, and J. Wilcox, *Mercury adsorption on PdAu, PdAg and PdCu alloys.* Main Group Chemistry, 2008. **7**(3): p. 205-215.
16. Zhao, H., et al., *Hg0 capture over CoMoS/γ-Al2O3 with MoS2 nanosheets at low temperatures.* Environmental Science & Technology, 2015.
17. Jung, J.-E., et al., *First-Principles Investigation of Mercury Adsorption on the α-Fe2O3(1$\bar{1}$02) Surface.* The Journal of Physical Chemistry C, 2015. **119**(47): p. 26512-26518.
18. Scala, F., C. Anacleria, and S. Cimino, *Characterization of a regenerable sorbent for high temperature elemental mercury capture from flue gas.* Fuel, 2013. **108**: p. 13-18.
19. Lim, D.-H. and J. Wilcox, *Heterogeneous Mercury Oxidation on Au(111) from First Principles.* Environmental Science & Technology, 2013. **47**(15): p. 8515-8522.
20. Sasmaz, E. and J. Wilcox, *Mercury Species and SO2 Adsorption on CaO(100).* The Journal of Physical Chemistry C, 2008. **112**(42): p. 16484-16490.
21. Wdowin, M., et al., *Experimental study of mercury removal from exhaust gases.* Fuel, 2014. **128**(0): p. 451-457.
22. Wiatros-Motyka, M.M., et al., *High capacity co-precipitated manganese oxides sorbents for oxidative mercury capture.* Fuel, 2013. **109**(0): p. 559-562.
23. Chhowalla, M., et al., *The chemistry of two-dimensional layered transition metal dichalcogenide nanosheets.* Nat Chem, 2013. **5**(4): p. 263-275.
24. Zhao, H., et al., *Hg0 Capture over CoMoS/γ-Al2O3 with MoS2 Nanosheets at Low Temperatures.* Environmental Science & Technology, 2016. **50**(2): p. 1056-1064.
25. Xie, J., et al., *Defect-Rich MoS2 Ultrathin Nanosheets with Additional Active Edge Sites for Enhanced Electrocatalytic Hydrogen Evolution.* Advanced Materials, 2013. **25**(40): p. 5807-5813.
26. Xiao, Z., et al., *Edge-selectively phosphorus-doped few-layer graphene as an efficient metal-free electrocatalyst for the oxygen evolution reaction.* Chemical Communications, 2016. **52**(88): p. 13008-13011.
27. Wang, Y., et al., *Porous cobalt-iron nitride nanowires as excellent bifunctional electrocatalysts for overall water splitting.* Chemical Communications, 2016. **52**(85): p. 12614-12617.
28. Tao, L., et al., *Edge-rich and dopant-free graphene as a highly efficient metal-free electrocatalyst for the oxygen reduction reaction.* Chemical Communications, 2016. **52**(13): p. 2764-2767.
29. Tao, L., et al., *Plasma-engineered MoS2 thin-film as an efficient electrocatalyst for hydrogen evolution reaction.* Chemical Communications, 2015. **51**(35): p. 7470-7473.
30. He, J., et al., *Modulation of surface structure and catalytic properties of cerium oxide nanoparticles by thermal and microwave synthesis techniques.* Applied Surface Science, 2017. **402**: p. 469-477.
31. Hu, X., et al., *Microwave-assisted preparation of flower-like cobalt phosphate and its application as a new heterogeneous Fenton–like catalyst.* Applied Surface Science, 2017. **396**: p. 1393-1402.
32. Voiry, D., et al., *High-quality graphene via microwave reduction of solution-exfoliated graphene oxide.* Science, 2016.
33. Fang, L., et al., *Growth of graphene on Cu foils by microwave plasma chemical vapor deposition: The effect of in-situ hydrogen plasma post-treatment.* Applied Surface Science, 2016. **383**: p. 28-32.
34. Sari, F.N.I. and J.-M. Ting, *One step microwaved-assisted hydrothermal synthesis of nitrogen doped graphene for high performance of supercapacitor.* Applied Surface Science, 2015. **355**: p. 419-428.

35. Hu, H., et al., *Compressible Carbon Nanotube–Graphene Hybrid Aerogels with Superhydrophobicity and Superoleophilicity for Oil Sorption.* Environmental Science & Technology Letters, 2014. **1**(3): p. 214-220.
36. Zhao, H., et al., *Hg0-temperature-programmed surface reaction and its application on the investigation of metal oxides for Hg0 capture.* Fuel, 2016. **181**: p. 1089-1094.
37. Lee, C., et al., *Anomalous Lattice Vibrations of Single- and Few-Layer MoS2.* ACS Nano, 2010. **4**(5): p. 2695-2700.
38. Zhao, H., et al., *Recovery of elemental sulphur via selective catalytic reduction of SO2 over sulphided CoMo/γ-Al2O3 catalysts.* Fuel, 2015. **147**: p. 67-75.
39. F. Ortmann, F. Bechstedt, and W. G. Schmidt, *Semiempirical van der Waals correction to the density functional description of solids and molecular structures.* Physical Review B, 2006. **73**(20): p. 205101.
40. D. Vanderbilt, *Soft self-consistent pseudopotentials in a generalized eigenvalue formalism.* Physical Review B, 1990. **41**(11): p. 7892-7895.
41. H. J. Monkhorst and J. D. Pack, *Special point for Brillouin-zone integratuibs.* Physical Review B, 1976. **13**(12): p. 5188-5192.
42. Li, S.-L., et al., *Quantitative Raman Spectrum and Reliable Thickness Identification for Atomic Layers on Insulating Substrates.* ACS Nano, 2012. **6**(8): p. 7381-7388.
43. Zhang, G., et al., *Two-dimensional layered MoS2: rational design, properties and electrochemical applications.* Energy & Environmental Science, 2016. **9**(4): p. 1190-1209.
44. Atkins, P.W., *Physical Chemistry*. The extent of adsorption. 2001, Oxford University Press.
45. Y. Wang, et al., *First-principles study of transition-metal atoms adsorption on MoS2 monolayer.* Physica E: Low-dimensional Systems and Nanostructures, 2014. **63**: p. 276-282.